# Dynamics of the O plus ClO Reaction: Reactive and Vibrational Relaxation Processes

**ARTICLE** *in* THE JOURNAL OF PHYSICAL CHEMISTRY A · NOVEMBER 2014

Impact Factor: 2.69 · DOI: 10.1021/jp511498r



**5 AUTHORS**, INCLUDING:

Pedro J. S. B. Caridade

University of Coimbra

**38** PUBLICATIONS **448** CITATIONS

SEE PROFILE

Antonio J. C. Varandas

University of Coimbra

**382** PUBLICATIONS **6,750** CITATIONS

SEE PROFILE

THE JOURNAL OF PHYSICAL CHEMISTRY A

Article

pubs.acs.org/JPCA

# Dynamics of the O + ClO Reaction: Reactive and Vibrational Relaxation Processes

O. B. M. Teixeira,[†] P. J. S. B. Caridade,*[,‡,¶] V. C. Mota,[§] J. M. Garcia de la Vega,[†] and A. J. C. Varandas*[,‡,§]

[†]Departamento de Química Física Aplicada, Universidad Autónoma de Madrid, 28049 Madrid, Spain

[‡]Centro de Química, and Departamento de Química, Universidade de Coimbra, 3004-535 Coimbra, Portugal

[¶]Instituto de Investigação Interdisciplinar, Universidade de Coimbra, 3030-789 Coimbra, Portugal

[§]Departamento de Física, Universidade Federal do Espírito Santo, 29075-910 Vitória, Brazil

**ABSTRACT:** Classical trajectories have been integrated to study the O + ClO reaction, both reactive and vibrational energy transfer processes, for the range of temperatures $100 \leq T/\mathrm{K} \leq 500$ using momentum Gaussian binning. The employed potential energy surface is the recently proposed single-sheeted double many-body expansion potential energy surface for the $^2A''$ ground-state of $ClO_2$ based on multireference ab initio data. A capture-type regime with a room-temperature rate constant of $(17.8 \pm 0.5) \times 10^{-12}$ cm$^3$ s$^{-1}$ and temperature dependence of $k(T/\mathrm{K})/\mathrm{cm}^3\ \mathrm{s}^{-1} = 22.4 \times 10^{-12} \times T^{-0.81} \exp(-39.2/T)$ has been found. Although the value reported here is half of the experimental and recommended one, tentative explanations are given. Other dynamical attributes are also examined for the title reaction, with state-to-all and state-to-state vibrational relaxation and excitation rate constants reported for temperatures of relevance in stratospheric chemistry.

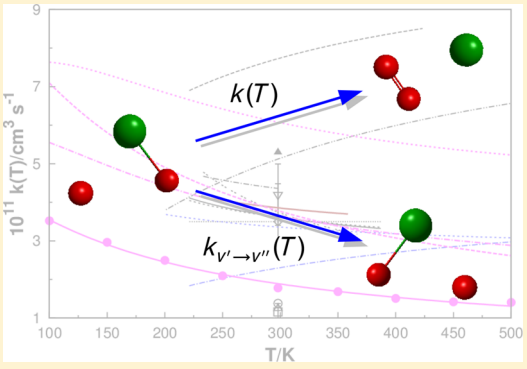


## 1. INTRODUCTION

During the 1960s, improved laboratory measurements have shown that pure-oxygen reactions could not explain the abundances of atmospheric ozone in the upper-stratosphere through the so-called Chapman mechanism. Additional processes were required, bearing in mind that the number of constituents in that atmospheric region is limited. Bates and Nicolet[1] proposed that trace constituents could be the missing clue. However, because they are in trace concentrations, they would be rapidly consumed, and hence such a limitation could only be overcome if they could participate in a catalytic cycle capable of regenerating them at the end of the process. One possibility would be the catalytic cycle:[2]

$$\mathrm{Cl} + \mathrm{O_3} \rightarrow \mathrm{ClO} + \mathrm{O_2} \quad (1)$$

$$\mathrm{O} + \mathrm{ClO} \rightarrow \mathrm{Cl} + \mathrm{O_2} \quad (2)$$

$$\mathrm{Net:\ O} + \mathrm{O_3} \rightarrow 2\mathrm{O_2} \quad (3)$$

with reaction 2 being the exothermic rate-determining step in the chlorine-catalyzed destruction of ozone, as illustrated in Figure 1. Using such a concept, Molina and Rowland[3] have shown that perturbations in the ozone layer in the Antarctic stratosphere[4] could be attributed to the release of chlorofluorocarbons, due to the presence of chlorine radicals in the cycle defined by eqs 1 and 2). Accordingly, the reactions 1 and 2 are crucial for calculating the ozone concentration and make predictions of the evolution of the stratospheric ozone layer.

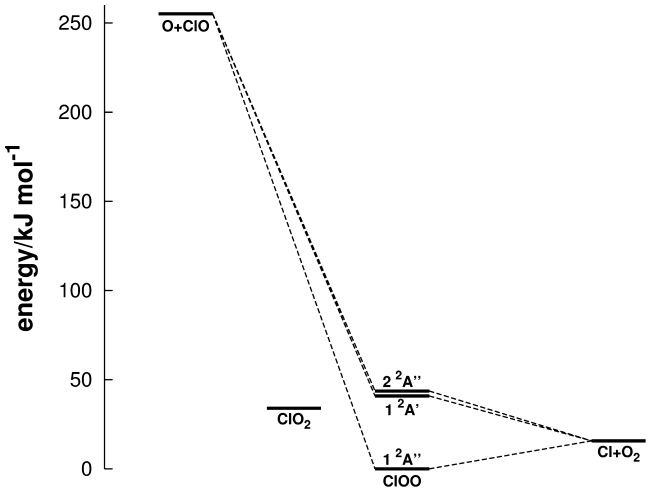


**Figure 1.** Energetics of the title reaction as calculated at the optimized MRCI/*VDZ* geometry of ClOO.

Numerous experimental studies have focused on reaction 2 to obtain the thermal rate constant and temperature dependence. Early indirect values[5−7] pointed to a room-temperature rate constant of $(1.16–1.25) \times 10^{-11}$ cm$^3$ s$^{-1}$, but direct

**Received:** November 17, 2014
**Published:** November 28, 2014

   dx.doi.org/10.1021/jp511498r | *J. Phys. Chem. A* 2014, 118, 12120−12129

measurements using discharge-flow/resonance fluorescence[8,9] indicated a value almost 5 times larger and the presence of an activation barrier. More recently, experimental results[10−14] point to rate constant values between 3.5 to 4.2 × $10^{-11}$ $cm^3$ $s^{-1}$ with no activation barrier and almost independent of temperature and pressure. In 2001, Golfarb et al.[15] reported a study using a discharge flow tube coupled to a pulse laser photolysis−atomic resonance fluorescence apparatus covering the range 227 to 362 K. The value of 3.9 × $10^{-11}$ $cm^3$ $s^{-1}$ is probably the most accurate result. In fact, Golfarb et al.[15] recommends the value of 3.7 × $10^{-11}$ $cm^3$ $s^{-1}$, probably in line with the Atkinson et al.[16] and Sanders et al.[17] recommendations.

Theoretically, only two studies are reported in the literature. Jaffe[18] studied the potential energy surface (PES) for the $^2A''$ ground-state and performed dynamics studies using the quasiclassical trajectory (QCT) method, with a thermal rate constant of 2.3 × $10^{-11}$ $cm^3$ $s^{-1}$ being reported, which is about half of the experimental and recommended value for reaction. In turn, Zhu and Lin[19] studied the isomerization and decomposition of the $ClO_2$ radical using density functional theory (DFT) and computed rate constants within the microcanonical variational RRKM method. Clearly, their approach ignores any nonstatistical recrossing effects, an issue also discussed in this work. Moreover, reaction 2 has been determined indirectly using the rate of reaction followed by dissociation, with the proposed rate constant being 3.7 × $10^{-11}$ $cm^3$ $s^{-1}$ and a negative temperature dependence observed, both in good agreement with the most recent experimental data.

To study the title reaction, the electronic correlation rules state that the entire manifold that correlates with both reagents and products should be considered. Of them, the 1 $^2A''$ electronic state of $ClO_2$ is the most stable and hence the one that is expected to contribute mostly to the reaction rate constant. Nevertheless, Jaffe[18] pointed out the important role of 1 $^2A'$ excited electronic state to obtain accurate results. Recently, a global single-sheeted double many-body expansion (DMBE) potential energy surface has been reported for the 1 $^2A''$ state of $ClO_2$ based on 3200 ab initio points calculated at MRCI/cc-pV*D*Z and *T*Z levels of theory and subsequently CBS extrapolated to the limit of an infinite-zeta basis.

The major goal of the present work is to perform dynamics calculations on the recently reported DMBE PES of ground-state $ClO_2$ with a view to study the reaction rate and vibrational relaxation in the O + ClO collisional process of eq 2. The paper is organized as follows: section 2 sketches the most relevant aspects related to the electronic structure of the $ClO_2(1\ ^2A'')$ ab initio-based DMBE form. In section 3, the quasiclassical trajectory[20] method is described, in particular by employing a variant known as the momentum Gaussian binning[21] (MGB) technique to be discussed later. The dynamics and kinetics calculations for the O + ClO reaction are reported in section 4, and the vibrational relaxation study is reported in section 5. Some concluding remarks are gathered in section 6.

## 2. POTENTIAL ENERGY SURFACE

Because the correlation rules of the title reaction have been discussed in detail by Jaffe,[18] only the most relevant issues for the present work are recalled here. It is well established[22] that $O(^3P_g)$ correlates in $C_s$ symmetry with A′ + (2)A″ states, while the $\Pi$ state of $ClO(X\ ^2\Pi)$ transforms as A′ + A″. Combining the spin states of the two reactants, one then gets the other 6, $(3)^{2,4}$ A′ + $(3)^{2,4}$A″. Due to the high energy positioning of the quartet states[18] of ClOO, only the doublets should be relevant for the present work. In turn, for the $Cl(^2P_u)$ + $O_2(X^3\Sigma_g^-)$ reaction, the $P_u$ state of the chlorine atom correlates in $C_s$ symmetry with (2)A′ + A″ while $\Sigma_g^-$ gives A″ states, thence yielding six states (three quartets and three doublets) with A′ + (2)A″ symmetries. Neglecting spin−orbit coupling, it then follows that the reaction $O(^3P) + ClO(^2\Pi) \rightarrow Cl + O_2(^3\Sigma_g^-)$ may occur on the 1 $^2A''$, 1 $^2A'$, and 2 $^2A''$ potential energy surfaces of ClOO in relative order of likelihood. Of these, only the 1 $^2A''$ PES has a stable $C_{2v}$ minimum which has been widely described in the literature.[23]

Recently,[24] an ab initio-based global PES has been proposed for the ground electronic state (1 $^2A''$) using the DMBE[25−29] method. This contains a realistic description of the long-range forces (as obtained for the electrostatic and dispersion interactions via damped multipolar expansions at both the reactant and product channels) which is inherent to the DMBE formalism.[25] Regarding the electrostatic interactions, which are expected to have a significant role in the $O(^3P) + ClO(^2\Pi)$ reaction, both contributions arising from the interaction of the permanent quadrupole moment of the oxygen atom and the permanent dipole and quadrupole moments of the chlorine oxide have been considered. In turn, the strong interaction region has been modeled via ab initio calculated energies using MRCI + Q method[30] and cc-pV*X*Z (*X* = *D* and *T*) basis set,[31,32] subsequently extrapolated to the CBS limit in what concerns the correlation energy with the two-parameter uniform singlet- and triplet-pair (USTE) protocol.[33] Besides performing with high accuracy when compared with the results from available explicitly correlated methods, especially in cases where bases with high cardinal numbers are affordable, an asset of USTE is that reliable CBS extrapolated energies are obtained even when cardinal numbers as small as *X* = *D* and *T* are utilized for the extrapolation. As far as the CASSCF energy is concerned, it has been CBS extrapolated using V*D*Z and V*T*Z energies and one of the Karton−Martin protocols,[34] which have been suggested for basis sets larger than triple-ζ, say V*T*Z and V*Q*Z. Because MRCI-Q calculations based on the latter basis would be unaffordable, the extrapolation of the CASSCF energy has been itself carried out using only V*D*Z and V*T*Z basis and the (*T*,*Q*) Karton−Martin scheme, with the accuracy of the procedure assessed a posteriori. Indeed, it has been shown that the errors associated with this (*D*,*T*) CBS extrapolation of the CASSCF energy were within the accuracy of the raw ab initio energies themselves. The overall PES fit to the total energies shows a root-mean squared deviation of only 4.7 kJ $mol^{-1}$ up to 4000 kJ $mol^{-1}$.

Figure 2 illustrates the DMBE PES[24] for $ClO_2(1\ ^2A'')$ as obtained in a relaxed triangular plot using hyperspherical coordinates.[35] These are defined as

$$\beta^* = \sqrt{3}(R_2^2 - R_3^2)P^{-1} \quad (4)$$

$$\gamma^* = (2R_1^2 - R_2^2 - R_3^2)P^{-1} \quad (5)$$

where $P = R_1^2 + R_2^2 + R_3^2$, and $R_1$ is the O−O distance. As it is visible from this plot, DMBE form predicts a minimum of $C_s$ symmetry which corresponds to a stable species whose minimum lies 15.5 kJ $mol^{-1}$ below the energy of the Cl + $O_2$ dissociation channel, hereafter named as $MC_s$ ($\beta^* = \pm 0.433$, $\gamma^* = -0.702$). Thus, it is nearly 4 kJ $mol^{-1}$ higher than the experimental value,[37] or 8 kJ $mol^{-1}$ higher if the spin−orbit coupling is included. Such a discrepancy, albeit any experimental errors, can be attributed to the necessity of


dx.doi.org/10.1021/jp511498r | J. Phys. Chem. A 2014, 118, 12120−12129

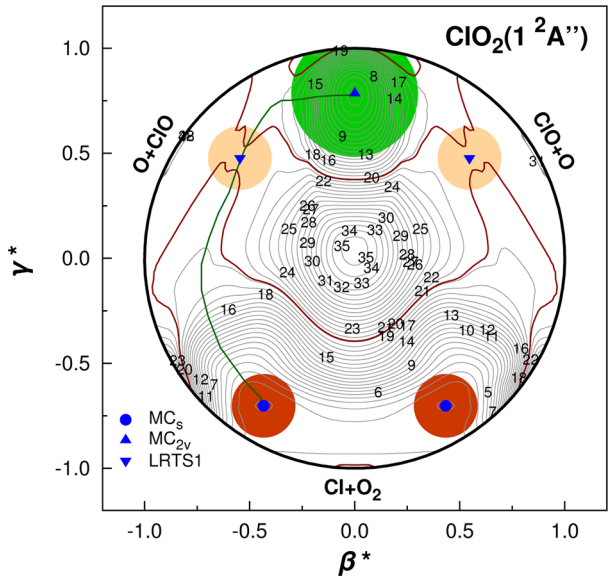


**Figure 2.** DMBE potential energy surface for $ClO_2(1\ ^2A'')$ using optimized hyperspherical coordinates.[35] The colored circles are regions relevant for dynamics (see text) centered in $C_s$ and $C_{2v}$ minimum, ($\beta^* = \pm 0.433$, $\gamma^* = -0.702$) and ($\beta^* = 0$, $\gamma^* = 0.784$), respectively, and saddle-point ($\beta^* = \pm 0.546$, $\gamma^* = 0.477$). Contours start at −504 kJ mol$^{-1}$ equally spaced by 13 kJ mol$^{-1}$, with a special contour (red) of −253 kJ mol$^{-1}$. The minimum energy path obtained by a simplified string method[36] is also shown connecting the $C_s$ and $C_{2v}$ structures.

including core effects and larger active spaces in the MRCI calculations, both computationally prohibitive[37] when generating the whole set of points required to model a global form. In turn, the structure located at ($\beta^* = 0.0$, $\gamma^* = 0.784$) corresponds to the $C_{2v}$ minimum ($MC_{2v}$), which lies 34 kJ mol$^{-1}$ above the $C_s$ geometry. In fact, the relative position of the $C_{2v}$ and $C_s$ minima has been the subject of some debate,[19,23] with the most recent predictions[24] following the trend displayed by the current DMBE potential energy surface.

Also shown in Figure 2 is the minimum energy path between the $C_s$ and $C_{2v}$ isomers, as obtained via a simplified string method.[36] Starting from the two structures in Cartesian coordinates, a string connecting the isomers is chosen and discretized into 20 pivots. The evolution of the string over time has then been evaluated using the fourth-order Runge−Kutta method in the parametrization via equal arc approach. The transition state between the two isomers has been identified to be the LRTS1 of ref 24, lying 1.3 kJ mol$^{-1}$ below the O + ClO channel and 238 kJ mol$^{-1}$ above the $C_s$ minimum.

## 3. DYNAMICS CALCULATIONS

The dynamics of the title reaction has been carried using the quasiclassical method as generally reviewed in ref 20 and implemented in the VENUS96[38] computer code. The equations of motion are integrated classically starting from a set of coordinates that mimic the restrictions imposed by the quantum nature of the vibrational and rotational states of the reactant molecules. Accordingly, the total thermal rate constant assumes the form

$$k(T) = g_e(T)\left(\frac{2}{k_B T}\right)^{3/2}\left(\frac{1}{\mu\pi}\right)^{1/2} Q_{vj}(T)^{-1} \times \sum_{vj}(2j+1)\exp\left(-\frac{E_{vj}}{k_B T}\right)\int_0^\infty E_{tr}\sigma^x(E_{tr})\exp\left(-\frac{E_{tr}}{k_B T}\right)dE_{tr} \quad (6)$$

where $k_B$ is the Boltzmann constant, $\mu$ is the reduced mass of the reactants, and $E_{vj}$ and $Q_{vj}$ are the rovibrational energy and partition function, respectively. Because the dynamics is carried out adiabatically on the 1 $^2A''$ sheet, the electronic degeneracy factor $g_e(T)$ is defined by.

$$g_e(T) = Q_{ClO_2(^2A'')} Q^{-1}_{O(^3P)} Q^{-1}_{ClO(^2\Pi)} \quad (7)$$

with the electronic partition functions assuming the form

$$Q_{ClO_2(^2A'')} = 2 \quad (8)$$

$$Q_{O(^3P)} = 5 + 3\exp(-227.8/T) + \exp(-326.6/T) \quad (9)$$

$$Q_{ClO(^2\Pi)} = 2 + 2\exp(-457.5/T) \quad (10)$$

and accounting for the fine structure of the $O(^3P)$[39] and $ClO(^2\Pi)$[40] species. In the low temperature regime, the limiting value of eq 7 is $g_e = 2/10$, which is obtained due to the fact that $O(^3P_2)$ (79%) and $ClO(^2\Pi_{3/2})$ (99%) are most populated. Similarly, at high energy regimes, $g_e(T) \rightarrow 2/36$. Notice that, even for $T$ = 1000 K, 77% of the population corresponds to $O(^3P_g) + ClO(^2\Pi_{3/2})$, with the remaining 23% being for $O(^3P_g) + ClO(^2\Pi_{1/2})$.

Using Monte Carlo method to solve the sampling of the translational energy[20] in eq 6, one obtains $E_{tr} = k_B T \ln(\xi_1\xi_2)$, where $\xi_1$ and $\xi_2$ are two random numbers obtained to specify the translational energy associated with each trajectory. To obtain an accurate and realistic rovibrational distribution, the following cumulative function was then considered:[41]

$$C(v, j; T) = \sum_{v'=0}\sum_{j'=0}(2j'+1)\exp(-E_{v'j'}/k_B T)Q_{vj}(T)^{-1} \quad (11)$$

The lower value of the rotational quantum state has been fixed at $j$ = 1 because $^2\Pi$ state of the ClO molecule is considered to be Hund's case (a).[42] In turn, the rovibrational energies have been determined by solving the electronic Schödringer equation for the diatomic fragment as represented by realistic EHFACE2U[26,43] curves. For each temperature and trajectory, the ($v$, $j$) state is then obtained when the condition $C(v, j; T) \geq \xi_3$ is fulfilled.

Replacing the sampling procedure in eq 6 for a set of $N$ integrated trajectories, the QCT thermal rate constant can be calculated by

$$k(T) = g_e(T)\left(\frac{8k_B T}{\pi\mu}\right)^{1/2}\pi b^2_{max} P_k \quad (12)$$

where $b_{max}$ is the maximum impact parameter, and $P_k = N_k/N$ is the probability of populating the $k$th channel. Statistically, 68% of associated error is then given by $\Delta k(T) = k(T)[(N - N_k)/(NN_k)]^{1/2}$, where $N_k$, in the above expressions, is the number of trajectories leading to the $k$th molecular arrangement.


dx.doi.org/10.1021/jp511498r | J. Phys. Chem. A 2014, 118, 12120−12129

**Table 1. Summary of the QCT-MGB Results for the Reactive Collisional Processes[a]**

| | | O + ClO | | Cl + $O_2$ | | | |
|---|---|---|---|---|---|---|---|
| $T$/K | $b_{max}$/Å | $P$ | $k(T)$ | $P$ | $k(T)$ | $k_{cap}(T)$ (rec) | $k_{cap,\langle C_4\rangle}(T)$ (rec) |
| 100 | 9.0 | 0.042 | 8.2 ± 0.3 | 0.18 | 35.2 ± 0.8 | 76.3(0.46) | 55.5(0.63) |
| 150 | 8.7 | 0.038 | 6.5 ± 0.4 | 0.15 | 29.7 ± 0.7 | 73.1(0.41) | 49.6(0.60) |
| 200 | 8.5 | 0.033 | 6.5 ± 0.4 | 0.13 | 24.9 ± 0.6 | 68.5(0.36) | 44.2(0.56) |
| 250 | 8.2 | 0.033 | 6.1 ± 0.3 | 0.11 | 21.0 ± 0.6 | 64.2(0.33) | 39.9(0.53) |
| 298 | 8.0 | 0.029 | 5.1 ± 0.3 | 0.10 | 17.8 ± 0.5 | 60.8(0.29) | 36.6(0.49) |
| 350 | 7.8 | 0.031 | 5.2 ± 0.3 | 0.10 | 16.8 ± 0.5 | 57.8(0.29) | 33.9(0.50) |
| 400 | 7.5 | 0.032 | 5.1 ± 0.3 | 0.10 | 15.1 ± 0.5 | 55.7(0.27) | 31.8(0.47) |
| 450 | 7.2 | 0.032 | 4.6 ± 0.3 | 0.10 | 14.2 ± 0.4 | 53.8(0.26) | 30.2(0.47) |
| 500 | 7.0 | 0.031 | 4.3 ± 0.2 | 0.10 | 14.1 ± 0.4 | 52.3(0.27) | 28.8(0.49) |

[a]Rate constants, in $cm^3\ s^{-1}$, multiplied by $10^{12}$. Also shown in parentheses are the recrossing ratios.

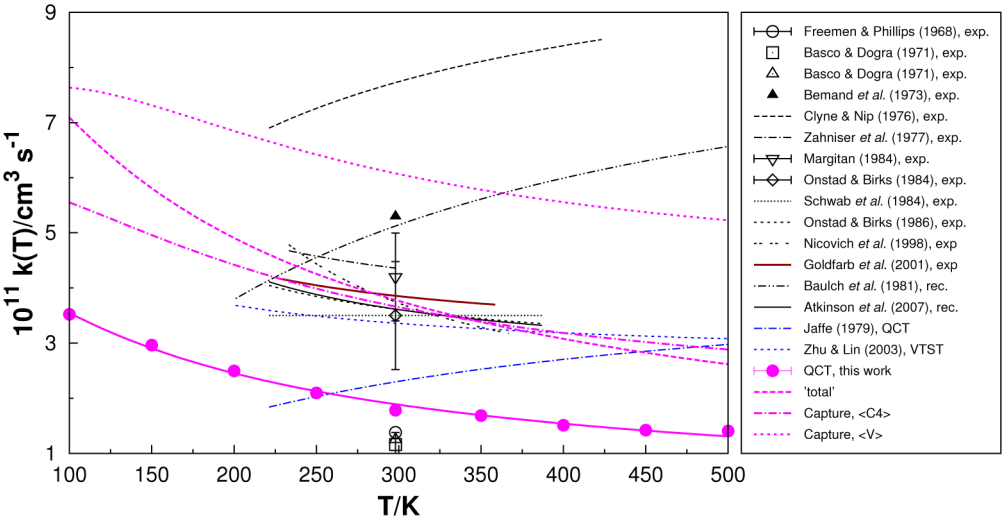


**Figure 3.** Temperature dependence of the Cl + $O_2$ formation rate constants using the QCT-MGB method and capture theory. Also reported are other theoretical results,[18,19] experimental[5−15,47] and recommended data.[16,17,48] The predition of the total rate constant (1 $^2A''$ and 1 $^2A'$) as twice the 1 $^2A''$ contribution is also shown.

One of the major flaws in the QCT method is the absence of internal energy quantization at the end of the trajectory due to zero-point energy leakage (ZPE);[21,44,45] see also references therein. Although the atoms considered in this work are heavy, thence favoring a classical treatment, an accurate description of the rovibrational states is required to obtain vibrational relaxation rate constants and internal energy distribution of the oxygen molecule. Several methods are discussed in the literature[44,45] to overcome ZPE and provide realistic rovibrational distributions. In the present work, we use the momentum Gaussian binning[21] (MGB) method, which is aimed to give an approximate, yet reliable, solution to both such issues. For the formed AB diatomic (either through reactive or nonreactive events), the rovibrational state $(v,j)$ probability is according to the MGB method given by

$$P_{vj}^{AB} = \sum_{i=1}^{N^{AB}} \frac{W_{vj}^{AB,(i)}}{N^{AB}} \tag{13}$$

where $W_{vj}^{AB,(i)} \sim W_{v}^{AB,(i)} W_{j}^{AB,(i)}$, and

$$W_k^i = \frac{1}{\rho_k \sqrt{\pi}} \exp\left[ -\left( \frac{\sqrt{E_k} - \sqrt{\varepsilon_k^i}}{\rho_k \sqrt{\overline{E}_k}} \right)^2 \right] \tag{14}$$

where $E_k$ is the $k$th diatomic energy eigenvalue, $\overline{E}_k$ is an average separation between neighboring channels, and $\varepsilon_k^i$ is the final energy (vibrational or rotational) of the $i$th trajectory. As usual in the traditional approach,[38] when the trajectory reaches a geometrical requirement for stopping, an additional 200 cycles are run to determine the averaged rotational energy. The vibrational component is then obtained as the residual part of the internal energy of the fragment. Recall now that the Gaussian-decay parameters act like fine-tuning constants, which are determined using the procedure reported elsewhere.[21] Using $\rho_v = 0.1$, the method should account for ZPE leakage because the contribution to the ground vibrational state of a trajectory ending with $\varepsilon_v^i = 0.9E_{v=0}$ turns out to be 48% of the value obtained with $\varepsilon_v^i = E_0$.[21] In turn, the determination of $\rho_j$ comes from the observation that the spacing of rotational levels is smaller than the vibrational ones. Accordingly, its value is fixed from the ratio of the averaged square-root of vibrational and rotational spacing, with the latter estimated by considering all vibrational states: $\rho_j = 0.1691$ for $O_2$ and $\rho_j = 0.2455$ for ClO.[21] It should be emphasized that the MGB differs from the GB[46] and very much behaves as expected from the theory. Indeed, the weights may be rationalized as reflecting the squared Gaussian dependence on the displacements from the square-root of the energy of a given contributing state to the


dx.doi.org/10.1021/jp511498r | J. Phys. Chem. A 2014, 118, 12120−12129

supposedly known classical value (viewed as the centroid of the relevant quantum distribution).[21]

The QCT-MGB rate constant can be calculated using the probabilities of eq 13, thence accounting for the ZPE of both the products and reactants. Assuming AB and BC as the diatomics fragments of reactants and products, the probability of BC formation can therefore be calculated as

$$P_{BC} = \frac{\sum_{vj}\sum_{i=1}^{N^{BC}} W_{vj}^{BC,(i)}}{\sum_{vj}\sum_{i=1}^{N^{AB}} W_{vj}^{AB,(i)}} \quad (15)$$

In turn, the thermal rate constant can be calculated using eq 6, while the statistical uncertainty (68% confidence level) in $k(T)$ is given by

$$\Delta k(T) = k(T)\left[\frac{\sum_{vj}\sum_{i=1}^{N^{AB}} W_{vj}^{AB,(i)} - \sum_{vj}\sum_{i=1}^{N^{BC}} W_{vj}^{BC,(i)}}{(\sum_{vj}\sum_{i=1}^{N^{AB}} W_{vj}^{AB,(i)})(\sum_{vj}\sum_{i=1}^{N^{BC}} W_{vj}^{BC,(i)})}\right]^{1/2} \quad (16)$$

## 4. REACTIVE COLLISIONAL PROCESSES

O + ClO → Cl + $O_2$ reaction is predicted by the DMBE potential energy surface to be exoergic by 239 kJ $mol^{-1}$ and driven by a barrier-free interaction leading to the ClOO minimum. In the present study, the dynamics has been carried out for the temperatures reported in Table 1 by integrating $10^4$ trajectories for each of them, thence in a number sufficiently large to warrant thermal rate constants converged within 1% for the dominant reactive process. The maximum impact parameter has been determined by running a small set of trajectories and checking if the last bin in the statistical analysis procedure for the reactive channel remained empty as it should. The temperature dependence of the QCT rate constant so calculated is visualized in Figure 3 where other theoretical,[18,19] experimental,[5−15,47] and recommended data[16,17,48] are also shown. In this table are also included the trajectories that lead to isomerization, i.e., to the exchange of an oxygen atom according to the reaction $O_a$ + $ClO_b$ → $O_b$ + $ClO_a$.

Theoretically, the first study of O + ClO reaction comes from the work of Jaffe[18] using QCT and phase space trajectory calculations. To construct the potential energy surface, Jaffe has utilized Morse potentials to describe the diatomic fragments and corrective forms for the bending and other topographical features. In turn, the coefficients have been made from spectroscopic data, with some of them being calibrated from dynamical properties. The thermal rate coefficient predicted from Jaffe's "best" reported potential energy surface is $k(T$ = 300 K) = 2.3 ± 0.2 × $10^{-11}$ $cm^3$ $s^{-1}$, thence only slightly larger than the one reported here (1.78 ± 0.05 × $10^{-11}$ $cm^3$ $s^{-1}$). Thus, the major difference encountered with Jaffe's work relates to the thermal dependence which he predicts to increase with temperature, thence implying that an activation energy[18] of 1.6 kJ $mol^{-1}$ is required, on average, for the reaction to occur.

To obtain an analytic representation of the QCT-MGB data, a generalized Arrhenius form has been employed:

$$k(T) = AT^m \exp(-B/T) \quad (17)$$

where the optimum numerical parameters are A = 223.292 × $10^{-11}$ $cm^3$ $s^{-1}$ $K^{-m}$, $m$ = −0.814383, and $B$ = 39.2058 $K^{-1}$. Clearly, eq 17 fits nicely the data over the entire range of temperatures considered here; see Figure 3. For a direct comparison with other results, a fit between 200 and 350 to the traditional Arrhenius function ($m$ = 0) has also been performed, yielding A = 9.65 × $10^{-12}$ $cm^3$ $s^{-1}$ and $Bk_B$ = $E_a$ = −1.6 kJ $mol^{-1}$. Although the value coincides with Jaffe's[18] prediction, the thermal rate coefficient in the present work decreases with temperature, suggesting a capture-like regime.

From the reported $b_{max}$ values in Table 1 and the shape of the rate constant in Figure 3, it is expected that the dynamics is dominated by long-range forces, as the latter decreases with increasing temperature. To progress on this, we need to obtain an estimate of the involved long-range interaction potential. As in similar cases previously considered,[49−51] two schemes have been used. The first is based on a fit of the spherically averaged O + ClO interaction DMBE potential energy surface to the effective long-range form

$$V_0(r) = -\langle C_n\rangle r^{-n} \quad (18)$$

where $\langle C_n\rangle$ and $n$ are nonlinear least-squares parameters, and $r$ is the distance between O and the center of mass of ClO. From a fit of the spherically averaged DMBE potential to eq 18 for $r$ > 1 Å, the following optimal least-squares parameters are obtained: $\langle C_n\rangle$ = 6046 kJ $mol^{-1}$ $Å^n$ and $n$ = 6.09. As the results suggest, the dominant contribution appears to arise from the leading dispersion term for $n$ = 6. Using eq 18, the capture rate constant is then given by[51,52]

$$k_{cap}(T) = g_e(T)\langle C_n\rangle^{2/n}\frac{2^{(3n-4)/2n}n\sqrt{\pi}}{(n-2)^{(n-2)/n}\sqrt{\mu}}\Gamma\left(\frac{2n-2}{n}\right)(k_BT)^{(n-4)/2n} \quad (19)$$

where $\Gamma(\cdots)$ is the ordinary gamma function. This yields the numerical values that are reported in Table 1 together with the corresponding recrossing factors predicted from $F_{rec} = k(T)/k_{cap}(T)$. As discussed elsewhere,[49] the recrossing can be of two types, statistical and nonstatistical, with the former not being expected to play any significant role in highly exoergic reactions. In turn, the nonstatistical recrossing may be identified with trajectories that enter the strong interaction region but do not form products. To highlight some details on the dynamics and recrossing, we have established three regions near the most important structures which are plotted in Figure 2 and analyzed the outcome of trajectories for $T$ = 298 K. It has been found that 29% of the nonreactive trajectories go through the region near the transition-state while only 2.5% enter the $C_s$ minimum region. It is then expected that the nonstatistical recrossing may be nearly 20−30% of the trajectories, corroborating the data of Table 1. An interesting feature in the isomerization is that all trajectories cross regions near the $C_{2v}$ minimum while 74% go through the long-range transition state (LRTS1). Regarding the reactive events, all trajectories undergo the $C_s$ minimum formation with only 2% passing through the $C_{2v}$ regions.

The second scheme utilized here to represent the spherically averaged long interaction potential is to consider only the leading term of the electrostatic interaction, $C_4$, as estimated using the classical optimized-quadrupole method.[53−56] This approach allows the quadrupole of the oxygen atom to adiabatically adjust at every geometry so that the electrostatic interaction is minimized. When replacing the optimum value of $C_4^{opt} = 0.59759e^2a_0^3$ in eq 19, one gets the rate constant reported in the last column of Table 1.

Recently, Zhu and Lin[19] reported a microcanonical variational RRKM study for the Cl + $O_2$ reaction. In their work, the

geometries of the involved species were computed at DFT level with the functional PW91PW91/6-311+G(3*d*, *f*), while the energies were obtained by the G2M method to approximate CCSDT/6-311-G(3*d* + *f*) level of theory. In turn, the O + ClO rate constant has been determined indirectly using the equilibrium constant for ClOO formation and the reverse rate constant. The predicted value at room temperature is $3.4 \times 10^{-11}$ cm$^3$ s$^{-1}$, which is pressure and temperature independent but nearly twice the QCT values. Both the modest level of theory used to calculate the PES and the use of statistical-type theories may partly explain the source of discrepancy with the global-dynamics results.

The number of experimental studies on the title reaction largely exceeds the theoretical predictions, although covering a wide range of room-temperature rate constants values. Three early studies[5−7] report indirect results for the O + ClO rate constant between 1.16 and $1.25 \times 10^{-11}$ cm$^3$ s$^{-1}$. In turn, direct measurements using discharge-flow/resonance fluorescence have been reported by Bemand[8] and Clyne and Nip[9] to be 5.3 and $5.2 \times 10^{-10}$ cm$^3$ s$^{-1}$, respectively, with the latter also presenting a study on the temperature dependence between 220 K and 426 K which suggests an activation barrier of $E_a$ = 0.8 kJ mol$^{-1}$. More recently, experimental results[10−14] point out to rate constant values between 3.5 to $4.2 \times 10^{-11}$ cm$^3$ s$^{-1}$ with no activation barrier, which are nearly temperature and pressure independent. In 2001, Golfarb et al.[15] reported a study using a discharge flow tube coupled to a pulse laser photolysis−atomic resonance fluorescence apparatus covering the range 227 K to 362 K. Of all estimates, $3.9 \pm 0.6 \times 10^{-11}$ cm$^3$ s$^{-1}$ is probably the most accurate value because the kinetics mechanism includes the formation of the ClO dimer at low temperatures.[57−59] Indeed, Golfarb et al.[15] recommend $3.7 \times 10^{-11}$ cm$^3$ s$^{-1}$ in line with Atkison's[16] recommendation.

It is clear from the previous paragraphs that QCT results are in poor agreement with the experimental data, although some show a large scatter. Clearly, the use of the spherically averaged potential produces rate constants nearly twice larger than QCT values. Of course, a major source for the discrepancy with the experimental results may be due to the neglect of the 1 $^2$A′ and 2 $^2$A″-state contributions. Assuming a similar topography, Jaffe estimated that the rate constant could be up to twice the value predicted from only the 1 $^2$A″ potential energy surface. If we consider valid such an assumption, the value from the present work would amount to $3.5 \times 10^{-11}$ cm$^3$ s$^{-1}$ at room temperature, which would lie within the error bars of the experimental and recommended values. Obviously, such an estimate must be confirmed not only by calculating and performing dynamics on 1 $^2$A′ and 2 $^2$A″ potential energy surfaces but also by taking into account the contribution of such excited states.

Figure 4 shows the rovibrational distribution for the newly formed oxygen molecules at three temperatures, $T$ = 100 K, 298 K, and 500 K, which are obtained by using the MGB method discussed in section 3. The major feature of such distributions is the highly vibrational outcome (up to $v$ = 16), with the maximum population occurring for $v$ = 12−14, a trend that is nearly temperature-independent. This may be explained by the conversion of potential energy into vibrational energy in the exoergic process of Cl + $O_2$ formation. Such behavior can be seen in Figure 5 where the total vibrational distribution is represented, showing an inverted population increasing almost linearly up to $v$ = 12. After reaching the maximum value of $v$, the amount of potential energy available (and kinetic energy

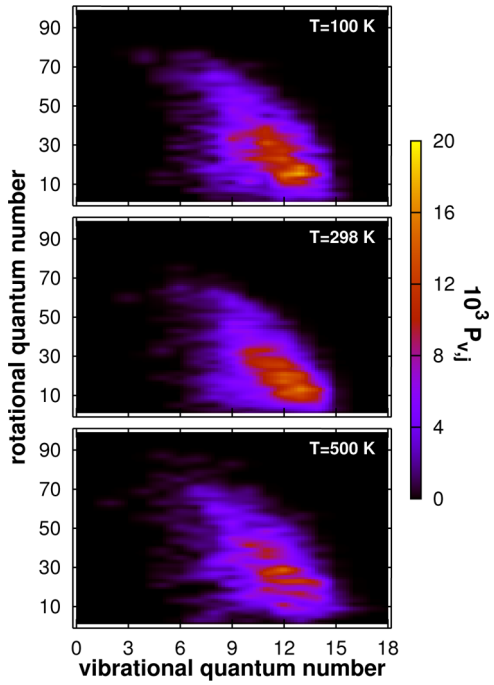


**Figure 4.** Rovibrational distributions of the newly formed $O_2(v',j')$ state for $T$ = 100 K, 298 K, and 500 K obtained using the MGB method.[21]

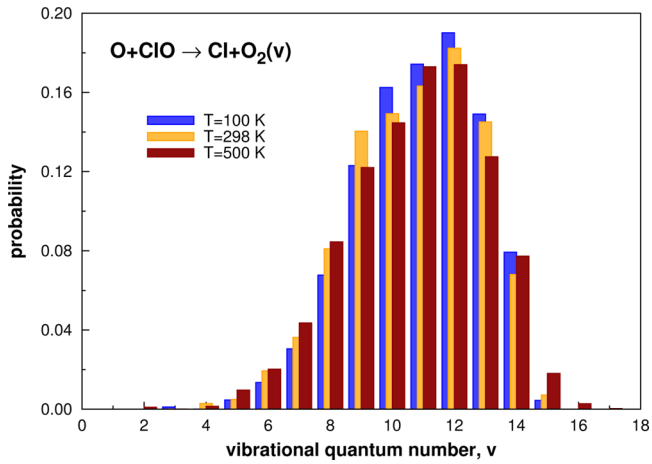


**Figure 5.** Total vibrational distribution of the oxygen molecule.

because we are dealing with low to moderate temperature regimes) for conversion diminishes, with a sharp decay being observed. Fixing the vibrational quantum state at the maximum value, $v$ = 12, we have obtained the rotational distribution shown in Figure 6, from which a Boltzmann regime can be anticipated. Plotting $\ln[P_{v=12,j'}/(2j' + 1)]$ as a function of the rotational energy, the rotational temperature is estimated to be 779 ± 39 K, 975 ± 61 K, and 1324 ± 175 K for $T$ = 100 K, 298 K, and $T$ = 500 K, respectively. The rotational temperature has linear behavior with temperature which may be attributed to an effective conversion of translational into rotational energy.

## 5. VIBRATIONAL RELAXATION OF CLO

The role of the vibrational relaxation of ClO is key when analyzing the kinetic processes of the title reaction because the radical is produced in collisions Cl + $O_3$ or Cl + $Cl_2O$. In atmospheric modeling if one assumes the local nonthermodi-


dx.doi.org/10.1021/jp511498r | J. Phys. Chem. A 2014, 118, 12120−12129

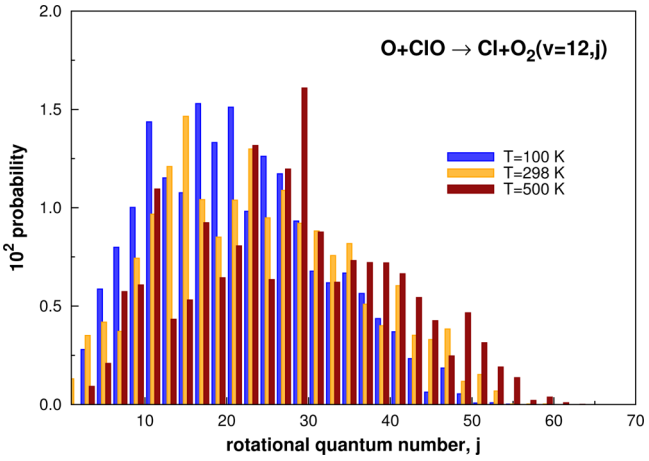


**Figure 6.** Rotational distribution of $O_2$ formation for $v' = 12$.

namical equilibrium to be valid, important reactions yield ClO vibrational excited states reaching up to $v = 7$. To assess the role of vibrational relaxation and produce a database that can be employed in network reactions, trajectories have been run for temperatures and initial vibrational states ($v'$) reported in Table 2. A total of 5000 trajectories have been integrated for each combination, using the thermalization of the translational energy and rotational quantum state, the trajectories being analyzed by the MGB method (considering both the nonreactive and O-exchange channels). The maximum impact parameter has been determined by binning procedure (as in reaction) for a small set of trajectories, leaving the bin $[19b_{max}/20{:}b_{max}]$ empty assuming the state-to-all vibrational relaxation process.

Figure 7 shows the state-to-all vibrational relaxation as a function of the initial quantum number. For the low temperature regime calculated, $T = 100$ K, the rate constant shows a bell-shaped behavior increasing from $v' = 1$ reaching a maximum at $v' = 5$. Although the translation energy for such temperature is sufficiently low to allow an effective vibrational randomization in the $C_{2v}$ minimum region, the probability of reaching this area is sufficiently low when vibrational excitation

**Table 2. Rate Constants for State-to-State, State-to-All Vibrational Relaxation, and State-to-All Vibrational Excitation Calculated Using $^2A''$ DMBE Potential Energy Surface**

| | | | | $10^{12}k_{v'\rightarrow v''}(T)$ | | | | | | | | |
|---|---|---|---|---|---|---|---|---|---|---|---|---|
| $v'$ | $b_{max}$/Å | $10^{12}k_{v'}^{dexc}(T)$ | $10^{12}k_{v'}^{exc}(T)$ | $v'' = 0$ | 1 | 2 | 3 | 4 | 5 | 6 | 7 | 8 |
| $T = 100$ K | | | | | | | | | | | | |
| 1 | 8.8 | 31 ± 1 | – | 31 | | | | | | | | |
| 3 | 8.4 | 41 ± 1 | – | 11.5 | 15.6 | 13.7 | | | | | | |
| 5 | 8.4 | 48 ± 1 | – | 11.6 | 12.4 | 8.8 | 7.4 | 8.0 | | | | |
| 7 | 8.6 | 47 ± 1 | 0.4 ± 0.1 | 10.5 | 7.1 | 6.0 | 5.5 | 5.3 | 6.9 | 6.1 | | |
| 9 | 8.8 | 45 ± 1 | 1.4 ± 0.2 | 7.6 | 5.9 | 4.2 | 3.8 | 4.7 | 5.4 | 4.1 | 4.8 | 4.3 |
| $T = 150$ K | | | | | | | | | | | | |
| 1 | 8.3 | 26 ± 1 | – | 26 | | | | | | | | |
| 3 | 8.2 | 34 ± 1 | – | 9.0 | 13.1 | 11.6 | | | | | | |
| 5 | 8.0 | 38 ± 1 | – | 8.9 | 9.4 | 6.6 | 7.3 | 6.1 | | | | |
| 7 | 8.3 | 39 ± 1 | 0.4 ± 0.1 | 8.4 | 6.0 | 4.7 | 4.5 | 3.9 | 6.0 | 6.0 | | |
| 9 | 8.4 | 40 ± 1 | 1.4 ± 0.2 | 6.9 | 4.3 | 3.5 | 3.4 | 4.5 | 4.1 | 4.9 | 4.3 | 3.8 |
| $T = 210$ K | | | | | | | | | | | | |
| 1 | 7.8 | 21.4 ± 0.8 | – | 21.4 | | | | | | | | |
| 3 | 7.9 | 26.7 ± 0.9 | – | 7.6 | 10 | 9.1 | | | | | | |
| 5 | 8.2 | 30 ± 1 | – | | 7.0 | 5.6 | 5.8 | 4.1 | | | | |
| 7 | 8.4 | 31 ± 1 | 0.4 ± 0.1 | 6.1 | 4.8 | 4.0 | 4.0 | 3.5 | 4.2 | 4.4 | | |
| 9 | 8.6 | 32 ± 1 | 1.6 ± 0.3 | 5.2 | 3.8 | 2.6 | 4.0 | 3.0 | 3.5 | 3.8 | 2.9 | 3.2 |
| $T = 298$ K | | | | | | | | | | | | |
| 1 | 7.5 | 17.6 ± 0.7 | 0.17 ± 0.08 | 17.6 | | | | | | | | |
| 3 | 7.5 | 22.8 ± 0.8 | 0.13 ± 0.07 | 6.7 | 8.8 | 7.3 | | | | | | |
| 5 | 7.5 | 24.5 ± 0.8 | – | 4.9 | 6.7 | 4.9 | 4.1 | 3.8 | | | | |
| 7 | 7.7 | 25.1 ± 0.9 | 0.4 ± 0.1 | 5.2 | 4.4 | 3.0 | 2.4 | 3.0 | 3.6 | 3.5 | | |
| 9 | 8.0 | 26.4 ± 0.9 | 1.5 ± 0.2 | 4.1 | 3.2 | 2.2 | 3.2 | 2.9 | 2.9 | 2.8 | 2.8 | 2.9 |
| $T = 350$ K | | | | | | | | | | | | |
| 1 | 7.5 | 13.5 ± 0.7 | 0.22 ± 0.09 | 13.5 | | | | | | | | |
| 3 | 7.5 | 19.2 ± 0.8 | – | 5.6 | 7.0 | 6.7 | | | | | | |
| 5 | 7.7 | 20.6 ± 0.8 | – | 4.1 | 5.4 | 4.0 | 3.7 | 3.3 | | | | |
| 7 | 8.0 | 23.0 ± 0.9 | 0.6 ± 0.1 | 4.1 | 4.3 | 3.3 | 2.1 | 2.9 | 3.1 | 3.3 | | |
| 9 | 8.2 | 23.8 ± 0.9 | 1.5 ± 0.2 | 3.1 | 2.7 | 1.8 | 2.1 | 2.5 | 3.2 | 3.5 | 2.1 | 2.8 |
| $T = 500$ K | | | | | | | | | | | | |
| 1 | 7.5 | 11.8 ± 0.6 | 0.6 ± 0.1 | 11.8 | | | | | | | | |
| 3 | 7.5 | 15.7 ± 0.7 | 0.26 ± 0.09 | 5.2 | 5.2 | 5.4 | | | | | | |
| 5 | 7.7 | 17.9 ± 0.8 | 0.18 ± 0.08 | 3.5 | 4.4 | 3.3 | 3.7 | 3.0 | | | | |
| 7 | 8.0 | 19.2 ± 0.8 | 0.6 ± 0.1 | 2.9 | 3.4 | 2.6 | 2.0 | 2.5 | 2.9 | 2.8 | | |
| 9 | 8.2 | 21.0 ± 0.9 | 1.7 ± 0.3 | 2.3 | 2.1 | 2.0 | 1.8 | 2.1 | 2.7 | 2.5 | 2.4 | 3.1 |


dx.doi.org/10.1021/jp511498r | J. Phys. Chem. A 2014, 118, 12120−12129

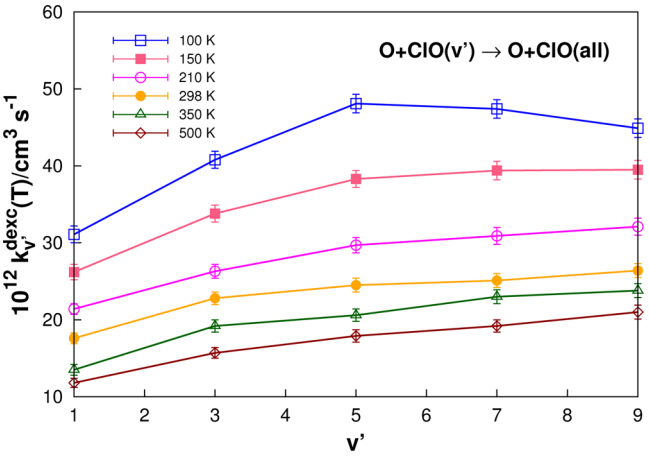


**Figure 7.** State-to-all vibrational relaxation rate constants as a function of the initial vibrational quantum state of ClO for the different temperatures studied.

is added, i.e., the shape of the entrance channel is sufficiently tight only to allow small $v'$. When increasing the temperature, the dependence with initial vibrational quantum state is linear and the role of the entrance channel shape diminishes, thus decreasing also the effectiveness of the energy transfer. The one-quantum vibrational relaxation is reported in Figure 8, showing exponential decay.

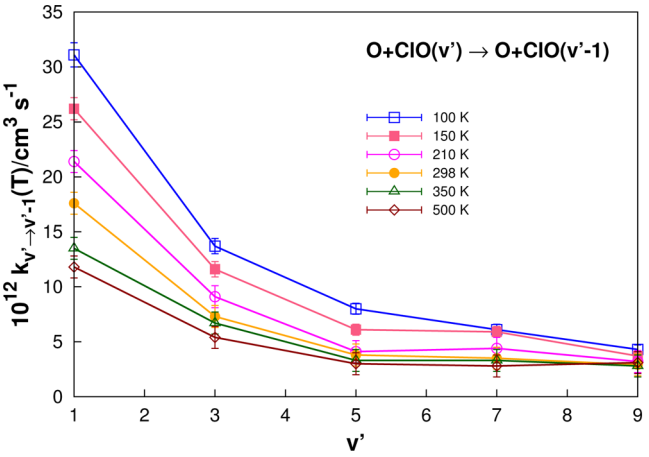


**Figure 8.** One-quantum vibrational relaxation rate constants: a function of the initial vibrational quantum state of ClO and temperature.

Multiquantum transitions have also been observed as shown in Figure 9 for $v' = 9$ at three temperatures. For high temperature regimes, one gets nearly uniform distribution over the final vibrational states, although the most populated are those involving one quantum. By decreasing the temperature, the role of internal randomization is observed, with the most probable transition being $v' = 9 \rightarrow v'' = 0$. In this case, the slow motion of the atoms due to low translation energy facilitates the energy transfer process.

Vibrational excitation has also been observed in the MGB-QCT results. For low temperatures, the diatomic ClO molecules show negligible vibrational excitations, which are 30 times smaller than in vibrational deactivation, and observed only for high vibrational states ($v' = 7$ and 9) where the energy separation between states becomes smaller. The excitation

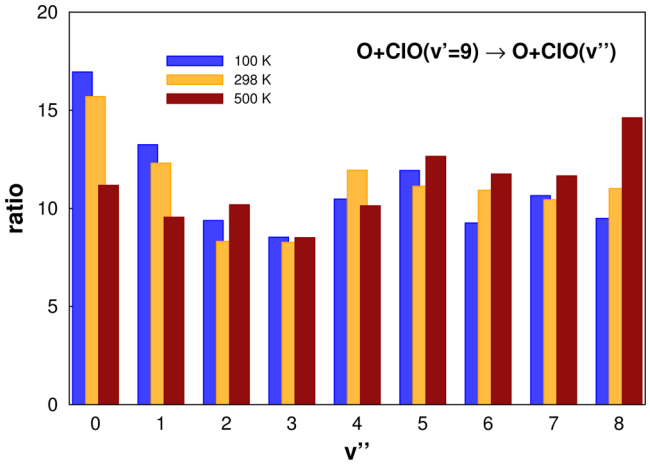


**Figure 9.** Multiquantum transition probability ($k_{v'\rightarrow v''}/\sum_{v''} k_{v'\rightarrow v''}$) for $v' = 9$.

process is temperature independent for $v' = 7$ and 9 while it increases with temperature for other $v'$. Notice the different trend when comparing vibration deactivation with excitation for high temperature regimes: an inverted, bell-shaped distribution with a minimum at $v' = 5$. Because it is expected that direct collisions predominate in the excitation process, trajectories with $v' = 5$ may sample regions of the potential energy surface that do not effectively transfer energy from translational to vibrational states.

## 6. CONCLUDING REMARKS

Is the discrepancy between experimental and theoretical work of O + ClO reaction a consequence of the accuracy of $ClO_2$ potential energy surface? Using a DMBE PES based on MRCI calculations, trajectories have been run showing that the contribution to the rate constant of the 1 $^2$A″ state is nearly half that of the reported experimental value. Despite the single-sheeted formalism used for the DMBE PES and the possible multistate nature of the process, we expect our theoretical study to be the most accurate so far available for the title reaction. Nevertheless, inclusion of the 1 $^2$A′ and 2 $^2$A″ states should be mandatory for obtaining an accurate thermal rate constant that is compatible with the experimental results. Thus, it may come as no surprise that the value of the rate constant obtained here is only about half of the experimental value. In fact, as suggested by Jaffe[18] based on the topographical similarities of the 1 $^2$A″ and 1 $^2$A′ PESs (as obtained from preliminary electronic structure calculations), a definitive answer can only be given by also using at least the 1 $^2$A′ PES, which is unfortunately not available in global form in the literature. The conclusions reached in the present work also pinpoint the necessity of including further electronic states in the study of the title reaction and hence provide a strong motivation for the calculation of the relevant analytic forms. However, even if such states are treated independently (i.e., by considering their separate contributions, each obtained using an adiabatic formalism similar to the one employed in the present work), the computational effort to calculate and fit the involved $ClO_2$ potentials plus their use in dynamics is a mammoth task that falls clearly beyond the scope of the present work. Work along such lines has been started and will hopefully be reported elsewhere.


dx.doi.org/10.1021/jp511498r | J. Phys. Chem. A 2014, 118, 12120−12129

Specifically, reactive rate constants determined using the MGB method have shown a typical capture regime that decreases with increasing temperature (which implies a negative barrier in the Arrhenius representation). By using capture theory, the reactive rate constant and nonstatistical recrossing factor have then been determined, which this has been found to be nearly 30%. In turn, by utilizing the recrossing estimate from the Zhu and Lin RRKM studies, their indirect value only based on the 1 $^2A''$ state DFT PES gives $2.3 \times 10^{-11}$ $cm^3$ $s^{-1}$ at room temperature. Clearly, there is good agreement with the QCT-MGB result reported here. Vibrational state-to-all and state-to-state rate coefficients have also been calculated for the first time for temperatures with relevance in stratospheric modeling. Multiquantum relaxation has been found to be the dominant process for all temperature regimes and initial vibrational quantum states.

## AUTHOR INFORMATION


### Corresponding Authors

*E-mail: pedrojcaridade@uc.pt.

*E-mail: varandas@uc.pt.


### Notes

The authors declare no competing financial interest.

## ACKNOWLEDGMENTS

O.B.M.T. thanks the University of Coimbra for various visits during the course of his studies. This work has the support of Fundação para a Ciência e a Tecnologia, Portugal (contracts PTDC/CEQ-COM3249/2012, PTDC/AAG-MAA/4657/2012, and SFRH/BPD/98132/2013), Ministerio de Ciencia e Innovación (MICINN), Spain (grant no. CTQ2010-19232), and the Brazilian funding agency Coordenação de Aperfeiçoamento de Pessoal de Nível Superior (CAPES). The support to the Coimbra Chemistry Centre through the project PEst-OE/QUI/UI0313/2014 is also gratefully acknowledged.

## REFERENCES


(1) Bates, D. R.; Nicolet, M. The photochemistry of atmospheric water vapor. *J. Geophys. Res.* **1950**, *55*, 301−327.

(2) Stolarski, R. S.; Cicerone, R. J. Stratospheric chlorine: A possible sink for ozone. *Can. J. Chem.* **1974**, *52*, 1610−1615.

(3) Molina, M. J.; Rowland, F. S. Stratospheric sink for chlorofluoromethanes: Chlorine atom-catalysed destruction of ozone. *Nature* **1974**, *249*, 810−812.

(4) Farman, J. C.; Gardiner, B. G.; Shanklin, J. D. Large losses of total ozone in Antarctica reveal seasonal $ClO_x/NO_x$ interaction. *Nature* **1985**, *315*, 207−210.

(5) Freeman, C. G.; Phillips, L. F. Kinetics of chlorine oxide reactions. I. The reaction of oxygen atoms with $Cl_2O$. *J. Phys. Chem.* **1968**, *72*, 3025−3028.

(6) Basco, S.; Dogra, N. Reactions of halogen oxides studied by flash photolysis. I. The flash photolysis of chlorine dioxide. *Proc. R. Soc. London A* **1971**, *323*, 29−68.

(7) Basco, S.; Dogra, N. Reactions of halogen oxides studied by flash photolysis. II. The flash photolysis of chlorine monoxide and of the ClO free radical. *Proc. R. Soc. London A* **1971**, *323*, 401−415.

(8) Bemand, P. P.; Clyne, M. A. A.; Watson, R. T. Reactions of chlorine oxide radicals. 4. Rate constants for reactions Cl+OClO, O+OClO, H+OClO, NO+OClO and O+ClO. *J. Chem. Soc., Faraday Trans. 1* **1973**, *69*, 1356−1374.

(9) Clyne, M. A. A.; Nip, W. S. Reactions of chlorine oxide radicals. Part 6 - The reaction O + ClO → Cl + $O_2$ from 220 to 426 K. *J. Chem. Soc., Faraday Trans. 1* **1976**, *72*, 2211−2217.

(10) Margitan, J. J. Kinetics of the reaction O + ClO → Cl + $O_2$. *J. Phys. Chem.* **1984**, *88*, 3638−3643.

(11) Schwab, J. J.; Toohey, D. W.; Brune, W. H.; Anderson, J. G. Reaction kinetics of O + ClO → Cl + $O_2$ between 252−347 K. *J. Geophys. Res.* **1984**, *89*, 9581−9587.

(12) Ongstad, A. P.; Birks, J. W. Studies of reactions of importance in the stratosphere. VI. Temperature dependence of the reactions O + $NO_2$ → NO + $O_2$ and O + ClO → Cl + $O_2$. *J. Chem. Phys.* **1984**, *81*, 3922−3930.

(13) Ongstad, A. P.; Birks, J. W. Studies of reactions of importance in the stratosphere. V. Rate constants for the reactions O + $NO_2$ → NO + $O_2$ and O + ClO → Cl + $O_2$ at 298 *K. J. Chem. Phys.* **1986**, *85*, 3359−3368.

(14) Nicovich, J. M.; Wine, P. H.; Ravishankara, A. R. Pulsed laser photolysis kinetics study of the O($^3$P) + ClO reaction. *J. Chem. Phys.* **1988**, *89*, 5670−5679.

(15) Goldfarb, L.; Burkholder, J. B.; Ravishankara, A. R. Kinetics of the O + ClO Reaction. *J. Phys. Chem. A* **2001**, *105*, 5402−5409.

(16) Atkinson, R.; Baulch, D. L.; Cox, R. A.; Crowley, J. N.; Hampson, R. F.; Hynes, R. G.; Jenkin, M. E.; Rossi, M. J.; Troe, J. Evaluated kinetic and photochemical data for atmospheric chemistry: Volume III - Gas phase reactions of inorganic halogens. *Atmos. Chem. Phys.* **2007**, *7*, 981−1191.

(17) Sander, S. P.; Abbatt, J.; Barker, J. R.; Burkholder, J. B.; Friedl, R. R.; Golden, D. M.; Huie, R. E.; Kolb, C. E.; Kurylo, M. J.; Moortgat, G. K. et al. *Chemical kinetics and photochemical data for use in atmospheric studies, Evaluation no. 17*; JPL Publication 10-6, Jet Propulsion Laboratory, Pasadena, 2011; http://jpldataeval.jpl.nasa.gov.

(18) Jaffe, R. L. Calculated rate constants for the reaction ClO + O → Cl + $O_2$ between 220 and 1000 K. *Chem. Phys.* **1979**, *40*, 185−206.

(19) Zhu, R. S.; Lin, M. C. Ab initio studies of $ClO_x$ reactions. VIII. Isomerization and decomposition of $ClO_2$ radicals and related bimolecular processes. *J. Chem. Phys.* **2003**, *119*, 2075−2082.

(20) Peslherbe, G. H.; Wang, H.; Hase, W. L. Monte Carlo sampling for classical trajectory simulations. *Adv. Chem. Phys.* **1999**, *105*, 171−201.

(21) Varandas, A. J. C. Trajectory binning scheme and non-active treatment of zero-point energy leakage in quasi-classical dynamics. *Chem. Phys. Lett.* **2007**, *439*, 386−392.

(22) Shuler, K. E. Adiabatic correlation rules for reactions involving polyatomic intermediate complexes and their application to the formation of OH($^2\Sigma^+$) in the $H_2$−$O_2$ flame. *J. Chem. Phys.* **1953**, *21*, 624−632.

(23) Peterson, K. A.; Werner, H. J. Multireference configuration interaction calculations of the low-lying electronic states of $ClO_2$. *J. Chem. Phys.* **1992**, *96*, 8948−8961.

(24) Teixeira, O. B.; Mota, V. C.; Garcia de la Vega, J. M.; Varandas, A. J. Single-sheeted double many-body expansion potential energy durface for ground-state $ClO_2$. *J. Phys. Chem. A* **2014**, *118*, 4851−4862.

(25) Varandas, A. J. C. A general approach to the potential energy functions of small polyatomic systems: Molecules and van der Waals molecules. *J. Mol. Struct.: THEOCHEM* **1985**, *120*, 401−424.

(26) Varandas, A. J. C. Intermolecular and intramolecular potentials: Topographical aspects, calculation, and functional representation via a DMBE expansion method. *Adv. Chem. Phys.* **1988**, *74*, 255−338.

(27) Varandas, A. J. C. Scaling of external correlation and analytical representation of potential energy surfaces: The general approach of the double many-body expansion. In *Trends in Atomic and Molecular Physics*; Yáñez, M., Ed.; Universidad Autonoma de Madrid: Madrid, 1990; p 113.

(28) Varandas, A. J. C. A new formulation of three-body dynamical correlation energy for explicit potential functions. *Chem. Phys. Lett.* **1992**, *194*, 333−340.

(29) Varandas, A. J. C. In *Lecture Notes in Chemistry*; Laganá, A., Riganelli, A., Eds.; Springer: Berlin, 2000; Vol. *75*; Chapter: Multivalued potential energy surfaces for dynamics calculations, pp 33−56.

(30) Werner, H.; Knowles, P. J. An efficient internally contracted multiconfiguration reference CI method. *J. Chem. Phys.* **1988**, *89*, 5803−5814.

(31) Dunning, T. H., Jr. Gaussian basis sets for use in correlated molecular calculations. I. The atoms boron through neon and hydrogen. *J. Chem. Phys.* **1989**, *90*, 1007−1023.
(32) Kendall, R. A.; Dunning, T. H., Jr.; Harrison, R. J. Electron affinities of the first-row atoms revisited. Systematic basis sets and wave functions. *J. Chem. Phys.* **1992**, *96*, 6796−6806.
(33) Varandas, A. J. C. Accurate global ab initio potentials at low-cost by correlation scaling and extrapolation to the one-electron basis set limit. *Chem. Phys. Lett.* **2007**, *443*, 398−407.
(34) Karton, A.; Martin, J. Comment on: "Estimating the Hartree−Fock limit from finite basis set calculations" [Jensen F (2005) Theor Chem Acc 113:267]. *Theor. Chem. Acc.* **2006**, *115*, 330−333.
(35) Varandas, A. J. C. A useful triangular plot of triatomic potential energy surfaces. *Chem. Phys. Lett.* **1987**, *138*, 455−461.
(36) E, W.; Ren, W.; Vanden-Eijnden, E. Simplified and improved string method for computing the minimum energy paths in barrier-crossing events. *J. Chem. Phys.* **2007**, *126*, 164103.
(37) Suma, K.; Sumiyoshi, Y.; Endo, Y.; Enami, S.; Aloisio, S.; Hashimoto, S.; Kawasaki, M. Equilibrium constants of the reaction of Cl with $O_2$ in the formation of ClOO. *J. Phys. Chem. A* **2004**, *39*, 8096−8099.
(38) Hase, W. L.; Duchovic, R. J.; Hu, X.; Komornicki, A.; Lim, K. F.; Lu, D.; Peslherbe, G. H.; Swamy, K. N.; Linde, S. R. V.; Varandas, A. J. C.; et al. VENUS96: A general chemical dynamics computer program. *QCPE Bull.* **1996**, *16*, 43.
(39) Moore, C. E. In *CRC series in evaluated data in atomic physics*; Gallagher, J. W., Ed.; CRC Press: Boca Raton, FL, 1993.
(40) Basco, N.; Morse, R. The vacuum ultraviolet absorption spectrum of ClO. *J. Mol. Spectrosc.* **1973**, *45*, 35−45.
(41) Caridade, P. J. S. B.; Varandas, A. J. C. Dynamics study of the $N(^4S) + O_2$ reaction and its reverse. *J. Phys. Chem. A* **2004**, *108*, 3556−3564.
(42) Gershnabel, E.; Shapiro, M.; Averbukh, I. S. Stern-Gerlach deflection of field-free aligned paramagnetic molecules. *J. Chem. Phys.* **2011**, *135*, 194310.
(43) Varandas, A. J. C.; Silva, J. D. Potential model for diatomic molecules including the united-atom limit and its use in a multiproperty fit for argon. *J. Chem. Soc., Faraday Trans.* **1992**, *88*, 941−954.
(44) Varandas, A. J. C. Excitation function for $H + O_2$ reaction: A study of zero-point energy effects and rotational distributions in trajectory calculations. *J. Chem. Phys.* **1993**, *99*, 1076−1085.
(45) Varandas, A. J. C. Four-atom bimolecular reactions with relevance in environmental chemistry: Theoretical work. *Int. Rev. Phys. Chem.* **2000**, *19*, 199−245.
(46) Bonnet, L.; Rayez, J. C. QCT: Weight binning. *Chem. Phys. Lett.* **1997**, *277*, 183−190.
(47) Zahniser, M. S.; Kaufman, F. Kinetics of the reactions of ClO with O and with NO. *J. Chem. Phys.* **1977**, *66*, 3673−3681.
(48) Baulch, D. L.; Duxbury, J.; Grant, S. J.; Montague, D. C. Evaluated kinetic data for high temperature reactions. Volume 4. Homogeneous gas phase reactions of halogen- and cyanide- containing species. *J. Phys. Chem. Ref. Data* **1981**, *10* (Supp. 1), 1.
(49) Varandas, A. J. C. Capture-energy-sudden plus recrossing model for atom-diatom reactions dominated by long range forces. Application to O + OH. In *Conferencias Plenarias de la XXIII Reunión Bienal de Química*; Feliciano, A. S., Grande, M., Casado, J., Eds.; Universidad de Salamanca: Salamanca, 1991; p 321.
(50) Silveira, D. M.; Caridade, P. J. S. B.; Varandas, A. J. C. Dynamics of the $O + OH_2$ reaction using two DMBE potential energy surfaces: The role of vibrational excitation. *J. Phys. Chem. A* **2004**, *108*, 8721−8730.
(51) Varandas, A. J. C. Accurate combined-hyperbolic-inverse-power-representation of ab initio potential energy surface for the hydroperoxyl radical and dynamics study of O plus OH reaction. *J. Chem. Phys.* **2013**, *138*, 134117.
(52) Le Roy, R. L. Relation between Arrhenius activation energies and excitation functions. *J. Phys. Chem.* **1969**, *73*, 4338−4344.
(53) Varandas, A. J. C. General discussion. *Faraday Discuss. Chem. Soc.* **1987**, *84*, 353−356.
(54) Varandas, A. J. C.; Brandão, J.; Quintales, A. M. A realistic $HO_2(\tilde{X}^2A'')$ potential energy surface from the double many-body expansion method. *J. Phys. Chem.* **1988**, *92*, 3732−3742.
(55) Varandas, A. J. C.; Rodrigues, S. P. J. Double many-body expansion potential energy surface for ground-state HCN based on realistic long range forces and accurate ab initio calculations. *J. Chem. Phys.* **1997**, *106*, 9647−9658.
(56) Rodrigues, S. P. J.; Varandas, A. J. C. On the variation of the electric quadrupole moment with internuclear distance and the atom−diatom long-range electrostatic interaction energy. *Phys. Chem. Chem. Phys.* **2000**, *2*, 435−439.
(57) Burkholder, J. B.; Hammer, P. D.; Howard, C. J.; Goldman, A. Infrared line intensity measurements in the $v = 0 - 1$ band of the ClO radical. *J. Geophys. Res.: Atmos.* **1989**, *94*, 2225−2234.
(58) Yokelson, R. J.; Burkholder, J. B.; Fox, R. W.; Ravishankara, A. R. Photodissociation of $ClONO_2$: 2. Time-resolved absorption studies of product quantum yields. *J. Phys. Chem. A* **1997**, *101*, 6667−6678.
(59) Kegley-Owen, C. S.; Gilles, M. K.; Burkholder, J. B.; Ravishankara, A. R. Rate coefficient measurements for the reaction OH + ClO → products. *J. Phys. Chem. A* **1999**, *103*, 5040−5048.